Journal of Spacecraft and Rockets
Vol. 48, No. 3, May–June 2011

Rotational Stiffness Study of Two-Element Tethered Coulomb Structures

Carl R. Seubert* and Hanspeter Schaub†
University of Colorado at Boulder, Boulder, Colorado 80309

DOI: 10.2514/1.49772

Combining features of large space structures and free-flying formations has lead to the tethered Coulomb structure concept. Using Coulomb forces to repel a formation of spacecraft nodes that are connected with fine tethers can create large quasi-rigid and lightweight space structures. There are numerous applications for a tethered Coulomb structure ranging from interferometry and remote sensing to component deployment and inflatable structures. This paper presents the first results of the impact of nodal attitude motions on the structure's dynamics and required charge levels. Nonlinear numerical simulations analyze the complex and coupled relative motion, and analytical natural frequency expressions are developed for small deflections. Quantitative analysis shows that for realistic kilovolt-level potentials, the inflationary Coulomb forces can stiffen the entire structure to resist deployment and external perturbations. This is demonstrated on a two-node system subject to initial angular-rate errors and differential solar radiation pressure. Further, a simple double-tether system is shown to offer increased stiffening properties and resistance to perturbations.

Nomenclature

A	=	linearized rotational response amplitude, rad
A_{braid}	=	tether braid cross-sectional area, m^2
A_s	=	reflective surface area, m^2
C_R	=	surface reflectivity constant
E	=	modulus of elasticity, Nm^{-2}
F_c	=	Coulomb force, N
F_{SRP}	=	solar radiation pressure force, N
F_s	=	tether spring force, N
I	=	mass moment of inertia, kgm^2
k_c	=	vacuum Coulomb constant, Nm^{2}C^{-2}
k_s	=	tether linear spring constant, Nm^{-1}
k_{s10}	=	nominal spring constant for 10 m separation, Nm^{-1}
L	=	tether length, m
L_e	=	equilibrium tether length, m
L_o	=	nominal tether length, m
m	=	node mass, kg
P_{SR}	=	solar radiation pressure, Nm^{-2}
Q	=	combined charge product, C^2
q	=	node charge, C
r	=	node spherical radius, m
t	=	time, s
V	=	node voltage, V
x	=	node separation, m
x_e	=	node equilibrium separation, m
x_o	=	node nominal separation, m
α	=	rotational oscillatory motion amplitude factor, N$^{1/2}$
α_{10}	=	rotational oscillatory motion amplitude factor for 10 m separation, N$^{1/2}$
β	=	linearized rotational response phase offset, rad
δL	=	tether stretch from nominal, m
δx	=	increase in node separation from equilibrium, m
δ_θ	=	node rotation from equilibrium, rad s^{-1}
θ	=	node angular rotation, rad
λ_d	=	Debye length, m
ϕ	=	double-tether attachment point half-angle, rad
ω_R	=	linearized rotational motion natural frequency, rad s^{-1}
ω_T	=	translational motion natural frequency, rad s^{-1}

Received 7 March 2010; revision received 10 December 2010; accepted for publication 17 January 2011.

*Graduate Research Assistant, Aerospace Engineering Sciences Department. Student Member AIAA.

†Associate Professor, H. Joseph Smead Fellow, Aerospace Engineering Sciences Department Associate Fellow AIAA.

I. Introduction

The use of spacecraft for remote sensing, interferometry, and telescopic operations is a growing area of research with large baselines sought to increase power, sensor accuracy and resolution. Large space structures and free-flying spacecraft formations are two active development approaches to address this need.

Large space structures offer rigid and fixed configurations, producing a precise sensor array platform for highly accurate observations. However, there are challenges to overcome before large space structures becoming standard operating systems, including large mass, volume, and cost constraints to get to orbit, the need for on-orbit construction or complexities and reliability of deployable components. Inflatable and deployable systems can offer a low-mass, high mechanical packaging efficiency, and potentially low-cost solution that can been used for applications such as antennas and booms [1–3]. An ongoing area of research is the development and test of deployable components and material membranes for large space structures [4].

An alternate method of providing the same characteristics of a large space structure is to use a cluster of spacecraft flying in a desired formation. The proposed NASA Stellar Imager [5] and the NASA study on the proposed Terrestrial Planet Finder [6] are two missions that intend to operate a formation of spacecraft creating a sensor baseline in the kilometer range. One of the leading applications of a large space interferometer is observations from geostationary Earth orbit (GEO). A study by Wertz [7] of a GEO-based free-flying formation indicates that an Earth surface resolution of 0.5–2 m is achievable. The eyeglass concept is another investigation into a GEO-based Earth surveillance platform with a 25–100 m aperture telescope. The diffractive lens is designed to be folded in a sequence similar to an origami layout and will be deployed in orbit [8,9]. King et al. [10] investigate the use of Coulomb forces to control a free-flying formation of spacecraft to develop a 20–30 m size array for interferometry at GEO.

One of the biggest challenges of a free-flying formation in Earth orbit is controlling the nonlinear and strongly coupled relative orbits and achieving the desired cluster geometry. With the use of conventional chemical thrusters there is a limitation of propellant and, consequently, mission lifetime to maintain a desired formation.

With close formations and sensitive instrument missions there are also plume impingement concerns. Two formation control concepts mitigating high fuel expenditure and plume impingement are electromagnetic [11] and flux pinning, both of which require high operational power levels [12]. Coulomb thrust is a recent and novel method to control the separation distance of spacecraft operating in close formations that does not have plume impingement concerns, is virtually propellantless, and requires only watt levels of power [10,13,14].

One potential solution to achieving a low-mass large space structure is with the tethered Coulomb structure (TCS) concept proposed in [13]. The TCS provides a hybrid combination of features from space structures and free-flying spacecraft formations. The TCS concept uses a formation of spacecraft nodes that are held together with a 3-D network of lightweight physical tethers. This is in contrast to other Coulomb spacecraft research that investigates the use of virtual tethers using electrostatic forces [15,16]. With the TCS concept each spacecraft node has the ability to increase its electrostatic potential through the use of a charge control device that emits either electrons or low-mass ions. With each node having the same charge polarity they will repel from each other and induce a tensile force on each tether. This Coulomb repulsive force essentially inflates the spacecraft structure, while the shape and size is maintained by the tethers. An illustration of a four-node TCS is shown in Fig. 1.

The TCS concept offers a number of advantages for the development of large space structures. Costs are kept low by launching the formation in a compact configuration that is inflated in orbit using the Coulomb forces. Similarly, a deployable component or antenna could essentially be inflated and held quasi-rigid from the spacecraft body using Coulomb force repulsion. Because of the micro- to millinewton levels of Coulomb force it is only necessary to have a network of fine, low-mass tethers. This significantly reduces the TCS mass compared with traditional structural components and does not require on-orbit construction. It is also envisioned that structures as large as hundreds of meters are feasible by connecting multiple charged nodes with relative short and thin tethers (tens of meters). Another key benefit of the concept is its ability to vary the shape and size of the TCS configuration by varying the tether lengths. This allows adaptability and variation for changing mission requirements.

There exists a variety of applications for space tether systems and studies typically use a spinning system [17,18], a gravity gradient or an atmospheric drag orientation to maintain tension [19,20]. A unique advantage of the TCS concept is that tension is provided with Coulomb forces regardless of the orbital orientation and can be used to overcome differential gravitational accelerations and external perturbations.

Controlling a free-flying spacecraft formation with Coulomb forces or traditional methods is an interesting dynamical challenge. On going research in this field includes equilibrium conditions of Coulomb craft [21,22], implementation of feedback stabilized virtual Coulomb structures with two craft [15,16,23], and the control of three craft [24,25]. The navigational and dynamical motion complexities of operating tightly controlled free-flying formations are significantly simplified with the TCS concept.

The TCS concept, with its many advantages, still requires further research to address the challenges; such as low-tension tether dynamics and deployment mechanisms, the dynamics of charged quasi-rigid structures with independently rotating nodes and variable TCS shape goals, the electrical power requirements to maintain nonequilibrium charge levels, as well as the ability to maintain a delicate TCS structure during orbital maneuvers such as semimajor-axis corrections. The intent of this paper is to investigate how increased nodal charge reduces attitude motions through enhanced rotational stiffness and the associated surface potentials required. The concern is that a node rotation due to small deployment errors, external torques or differential perturbations could cause the tethers to wind up or loose tension. This is an advancement over the previous TCS modeling that used point mass nodes (ignoring nodal attitude motions) and focused on how the overall structure motion and shape changes can be used to stabilize the TCS orientation [13].

Results are generated by numerically simulating the full nonlinear equations of motion for any general three-dimensional TCS size or shape using any number of spacecraft nodes. This algorithm development is shown in the Appendix. The presented results are a vital step for the future analysis of more complex systems and higher fidelity modeling of the TCS relative motion.

One core aspect throughout this study, is determining the conditions that cause periodic slack tethers with nominal configurations. It is desired that tethers do not reach a sufficiently slack state to cause tether damage or interference between nodes. However, the presence of slightly slack lines during short-term oscillations are not a strong concern.

The primary focus of this study is quantifying the ability of the Coulomb force to stiffen the overall TCS structure and resist deformation. To meet this objective, first, a study of the forces acting on a TCS system at GEO is given. A two-node numerical simulation is used to explore the capability of using charge to resist compression from differential external disturbance forces. The same two-node setup is then used to demonstrate the complex 3-D nonlinear motions that are anticipated.

The equations of motion of this two-node system are then reduced to 2 degrees of freedom (2DOF). This system is linearized to isolate translational and rotational motions and the corresponding natural frequencies are analyzed. This gives a measure of the rotational stiffness and the effects of varying model parameters.

Numerical simulations are then used to quantify the systems ability to resist initial angular-rate errors. These nonlinear simulations feature dynamic tethers modeled as simple, massless, proportional and undamped springs. Finally, to enhance the orientational stiffening capabilities of the Coulomb inflationary force, a TCS configuration with a redundant double-tether connection is investigated.

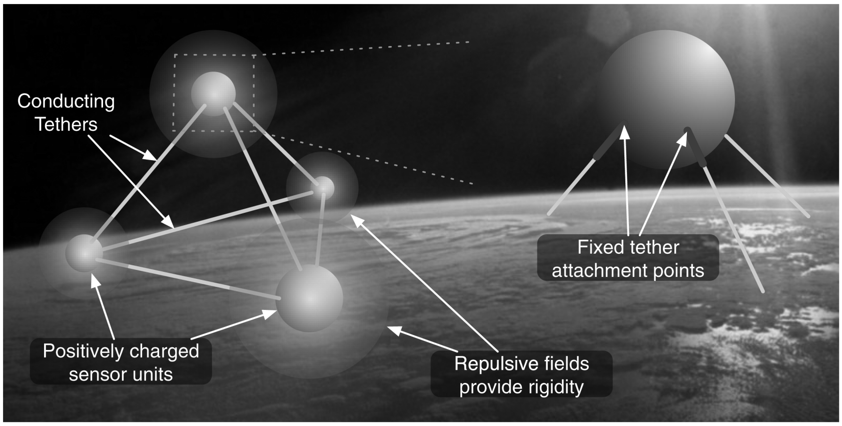

Fig. 1 Illustration of the tethered Coulomb structure concept.

This includes development of a 2DOF model and linearization analysis as well as comparing rotational stiffness to the single-tether system through numerical simulations.

II. Tethered Coulomb Structure Forces

This section develops the fundamental forces acting on a TCS system. The dynamic model considered includes translational and rotational degrees of freedom of each TCS node, Coulomb forces for inflation, and fixed, deployed tether lengths to maintain a constant average size and shape. The TCS shape will undergo small variations due to flexing of the tethers and motion of the nodes. A two-node TCS system is used to highlight the abilities of the Coulomb inflation to resist compression from a representative GEO disturbance force.

A. Coulomb Force

The Coulomb force is the controllable actuator for the TCS system. This force is generated from the interaction of two charged bodies. The charge can either occur naturally from the space plasma or be driven by a charge control device that continually emits charged particles. In space, the Coulomb force is reduced by shielding from the free-flying charged particles of the local plasma. The extent of this shielding is characterized by the Debye length λ_d [26]. The resulting space Coulomb force $\boldsymbol{F}_c$ that is generated between two craft of charges q_1 and q_2 is defined by

$$|\boldsymbol{F}_c| = k_c \frac{q_1 q_2}{x^2} e^{-x/\lambda_d}\left(1 + \frac{x}{\lambda_d}\right) \tag{1}$$

where x is the spacecraft separation distance and $k_c = 8.99 \times 10^9\ \mathrm{Nm^2\,C^{-2}}$ is the vacuum Coulomb constant. The Debye length is based on the temperature and density of the local plasma. At GEO the plasma is sufficiently hot and sparse to generate Debye lengths ranging from 80–1000 m with an average of approximately 200 m [10]. This allows the use of Coulomb thrust when operating with spacecraft separations of dozens of meters at GEO [14,27]. Low-Earth-orbit Debye lengths are typically cm level, making the use of Coulomb thrust challenging.

For TCS applications, the Coulomb force is chosen to be repulsive to provide an inflationary force to maintain tension on the tethers. This is achieved through a positive charge product, $Q = q_1 q_2$, with either both positive or negative q_i values. This study uses spherical spacecraft bodies, where a charge level q requires a surface potential computed with the relationship:

$$q = \frac{Vr}{k_c} \tag{2}$$

where V is the voltage and r is sphere radius. Note that this study does not consider nonhomogeneous charge distributions that can occur from induced charge effects of two neighboring conducting objects. Such effects are very small for separations greater than 5 sphere radii $x > 5r$. Also omitted from this study is the combined charge effect of having finite spheres in close proximity. The consequence is that for separations less than 10 sphere radii $x > 10r$, the craft would require a slightly higher surface potential to compensate for the minimal force reduction.

B. Tether Force

The tethers are modeled as linear stretch springs that go slack when in a compressed state, and no force is produced. Consequently, they only produce a force that opposes the repulsion of the Coulomb force. The magnitude of the force is governed by the equation

$$|\boldsymbol{F}_s| = \begin{cases} k_s \delta L & \delta L > 0, \\ 0 & \delta L \le 0 \end{cases} \tag{3}$$

where k_s is the linear spring constant and δL is the stretch in the tether length between two nodes. A linear spring tether is a suitable model for this study that is analyzing the relationship between translational and rotational motions with an emphasis on overall structural stiffening and disturbance rejection. The TCS algorithm is developed to allow future investigations to use more complex tether models that consider geometric deformations of the low-tension tether. However, the linear axial-stiffness model with nominal material property values provides an approximate measure of how well the two-node TCS could resist differential rotations.

Table 1 AmberStrand properties for three twisted fibers

Parameter	Value	Units
Modulus of elasticity E	9.5×10^9	$\mathrm{N/m^2}$
Cross-sectional area A_{braid}	5.6×10^{-7}	$\mathrm{m^2}$
Linear mass density	1.44	g/m

Table 2 Expected force magnitudes for a two-node TCS separated by 5 m

Force	Value	Units
Coulomb F_c	1.0	mN
Tether F_s	1.0	mN
SRP F_{SRP}	3.6	μN
Differential gravity	4.0	μN

One option for a spacecraft tether material is AmberStrand®.[‡] The property values of this reference material are used for all simulations in this paper. AmberStrand is an electrically conductive hybrid yarn made up of a metal-coated polymer that offers a flexible, low-mass and high strength tether. Tests conducted at the University of Colorado at Boulder on a braid of three twisted AmberStrand fibers resulted in the tether properties shown in Table 1.

The modulus of elasticity is measured in the elastic region of tensile test results. The modulus of elasticity is related to a linear spring constant in the elastic region of the stress-strain curve with

$$k_s = \frac{E A_{\mathrm{braid}}}{L_o} \tag{4}$$

where E is the modulus of elasticity, A_{braid} is the cross-sectional area of the braid of three twisted fibers, and L_o is the unstretched tether length.

C. Solar Radiation Pressure

At GEO, where the TCS concept is to be operated, solar radiation pressure (SRP) can play a significant role as a disturbance force on the inertial orbital motion of satellites [28]. For the TCS application the primary concern here is the effect of any differential SRP forces on short-term dynamics. A simplified SRP model is used to quantify the capability of the TCS system to compensate for a constant external perturbation. The magnitude of the SRP force acting on a spacecraft is governed by the relationship [29]

$$F_{\mathrm{SRP}} = P_{\mathrm{SR}} C_R A_s \tag{5}$$

where P_{SR} is the solar radiation pressure, C_R is the surface reflectivity constant of the spacecraft, and A_s is the surface area.

D. Sample Force Magnitudes

To appreciate the expected force magnitudes a TCS structure will encounter on orbit, consider a two-node tethered system. With nodes of radius 0.5 m, separated by 5 m center to center and charged to a surface potential of 30 kV the expected force levels are shown in Table 2. This is an achievable charge level. SPEAR-1 demonstrated controlled charge to 46 kV relative to the local plasma [30,31]. The Coulomb force is computed between two isolated point charges. The solar radiation pressure is computed for one node at 1 AU (astronomical unit) from the sun, where the solar radiation pressure is

[‡]Syscom Advanced Materials, Inc., www.amberstrand.com [retrieved 15 January 2010].

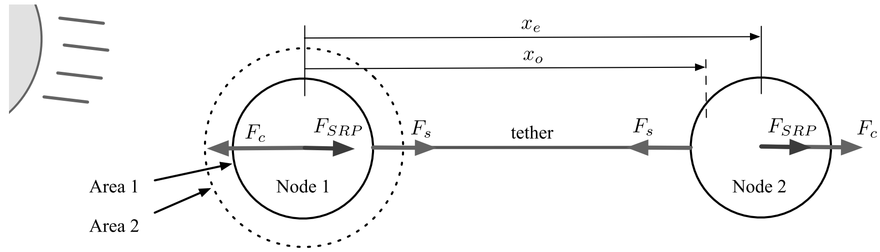

Fig. 2 Two-node Solar radiation pressure model.

4.56×10^{-6} N/m, and the surface reflectivity is 1. The differential gravity gradient force is computed assuming the nodes are aligned along the nadir line at GEO altitude, each with a mass of 50 kg.

In the absence of external perturbations (such as SRP or gravity gradients) there exists a force equilibrium between the Coulomb and tensile forces. Two nodes at 30 kV potential, with a desired separation ($x_o = 5$ m), using AmberStrand tether material need only stretch 0.75 μm to reach this equilibrium separation x_e.

E. Numerical Simulation: TCS Compression Because of External Disturbance Force

For this example TCS, the force magnitudes of the primary disturbances at GEO, differential SRP and differential gravity, are 3 orders of magnitude less than the Coulomb control forces. The intent of the following study is to quantify the capabilities of a two-node TCS configuration to resist deformation from an external perturbation, in this case, differential SRP.

Consider two spacecraft nodes connected with a single tether. The solar radiation pressure is added as a bias force that is compressing the system along the direction of the tether line, as shown in Fig. 2. The SRP force is acting on both nodes, but increasing the size of node 1 produces a differential SRP that attempts to compress the nodes. The concern is whether the Coulomb forces are large enough to maintain tether tension in this setup. The parameters of the study are shown in Table 3, and the simulation algorithm used is shown in the Appendix.

The nodes have a desired separation of 10 m. If the Coulomb forces are found to be sufficient to maintain tension for this challenging larger separation distance, then TCS systems of shorter separation distances should not be significantly compressed by differential SRP. The sunlit surface area of node 1 is increased linearly in multiples from 1 to 10, where one is the nominal surface area corresponding to a 0.5 m radius circle. An increase in the surface area will cause the homogeneously distributed charge to also increase for a fixed nodal potential. This would further increase the stiffening capabilities of the TCS system. To maintain a worst-case scenario, this model does not incorporate any change in the Coulomb force as the surface area of node 1 is increased. To isolate the differential solar radiation pressure effects, this simulation is run to not induce attitude rotations and omits gravity forces.

The numerical simulation is set up with the craft initially at their undisturbed equilibrium states. The contour plot of Fig. 3 shows what the worst-case percentage of the buffer between equilibrium distance and unstretched distance is compromised by the SRP disturbed relative motion. This value is calculated using

$$\% = \frac{L_e - \min(L)}{L_e - L_o} 100 \tag{6}$$

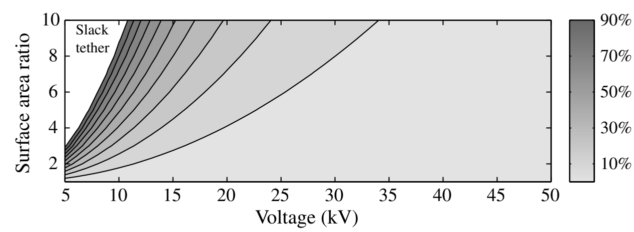

Fig. 3 Tether distance from becoming slack under varying SRP disturbances.

This percentage value indicates how close the tether length is from becoming slack as a function of both charge and the surface area ratio between the craft. The top left portion of the figure indicates that the crafts relative motion compresses to the point of causing the tether to go slack at times.

As indicated in Fig. 3 an increase in charge will stiffen the system to resist differential perturbations. For shorter separation distances of less than 10 meters the system is further stiffened reducing the voltage requirements to resist the same disturbance force levels. Note that even with a very large TCS node size ratio of 10 and 25 kV potential, the compression due to this worst-case alignment of the differential SRP disturbance would only cause approximately a 20% compression of the equilibrium distance buffer. For TCS separation distances on the meter level, considering near equal nodal sizes, the differential SRP will have a minimal impact on the TCS shape. Based on the results of this simulation it is appropriate to omit the effects of differential perturbations such as SRP and gravity to analyze short-term dynamical motions. For long-term dynamic studies, that are not performed here, the implementation of the full model in the appendix is used.

III. Two-Node Simulation Parameters

The intent of this paper is to provide insight into the dynamics and design parameters of the TCS concept. These studies are based upon the translational and rotational motion of a representative two-node system. The two-node system is subjected to initial angular-rate errors that represent deployment or disturbance torques.

Simulations are computed with the full three-dimensional equations of motion including attitude dependence, as detailed in the Appendix. For practical reasons, the simulations are stopped if an attitude reaches a tether wrap-up state (± 90 deg for a single tether). A common set of TCS parameters for each simulation case is shown in Table 4. Three unstretched separations of $x_o = 2.5$, 5, and 10 m measured from node center to center are used.

Table 3 Differential SRP numerical simulation parameters

Parameter	Value	Units
Spacecraft area ratios	1–10	
Spacecraft node radius r	0.5	m
Spacecraft separation x_o	10	m
Solar pressure (1 AU)	4.56×10^{-6}	Nm^{-2}
Surface reflectivity	1	

Table 4 TCS parameters common for all simulations

Parameter	Value	Units
Spacecraft node mass m	50	kg
Spacecraft node radius r	0.5	m
Spacecraft potential range V	5–50	kV
Spacecraft separations x_o	2.5, 5, 10	m
Initial attitude rate errors $\dot{\theta}(0)$	1–120	deg / min

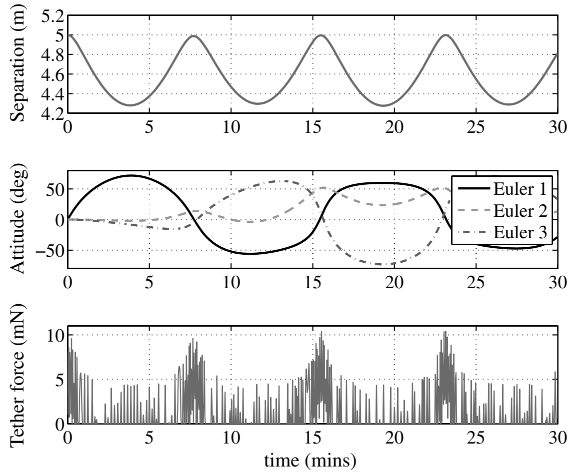

Fig. 4 Complex 3-D example of two-node relative motion, attitude, and single-tether tension (initial angular rates of 45 deg / min).

To demonstrate the complex coupling between translational and attitude motions of tethered, charged nodes an example simulation is shown. Figure 4 shows the relative motion of a two-node system in deep space. Each node has an initial angular rate of 45 deg / min about different axes. The nodes maintain a fixed potential of 30 kV and there are no gravity or SRP forces acting. The nodes have an unstretched separation of 5 m, radius of 0.5 m and mass of 50 kg. Figure 4 demonstrates the relative oscillatory motion of the two nodes along with the attitude of node 1 and the corresponding tether force levels.

Figure 4 indicates the complex dynamics that result from a two-node, single-tether TCS system with solely an initial angular-rate error. While this numerical simulation can handle general translational and rotational motion of N nodes, the results yield an overwhelming amount of data, making it difficult to gain any insight. This numerical demonstration highlights the need to reduce the complexity of the system. It is beneficial to isolate the motions of the TCS system and appreciate its true capabilities. For this reason, the following studies in this paper reduce a generic TCS system to its fundamental translational and rotational motions.

IV. Single-Tether Configuration Modeling

This section documents the dynamic model of the representative two-node, single-tether TCS system. This two-node model is reduced to two degrees of freedom and linearized to obtain insight into expected motions about equilibrium. The linearization allows specific analysis of individual translational and rotational motions. The models are developed in this section in the absence of gravitational and SRP perturbations. The two-degree-of-freedom models developed here also provide verification of the full 3-D model and simulation results.

A. Two-Degree-of-Freedom Model

A simplified 2DOF TCS model is developed to provide insight into how TCS node rotation impacts the charge requirements and related stiffness capabilities. This TCS model features two nodes attached with a single tether, as shown in Fig. 5.

By constraining the nodes to asymmetrically rotate by an angle θ the tether remains parallel to the line of sight vector resulting in one-dimensional translational motion with the Coulomb and tether forces (F_c and F_s) directly opposing each other. This reduces the model to one rotational and one translational degree of freedom. This motion is desirable as it allows analysis of the effects of each motion in isolation. Any alternate symmetries cause two-dimensional translational motions that are also inherently coupled to rotational motions. The Coulomb force for this model is assumed to have no shielding from the plasma environment due to the very small meter-level separation distances. This is a reasonable assumption, given the force magnitude is reduced only 0.03% at a separation of 5 m in a nominal 200 m Debye length plasma.

The translational equation of motion of this system is

$$\ddot{x} = \frac{2k_c Q}{mx^2} - \frac{2k_s}{m}[x - x_o + 2r(1 - \cos\theta)] \tag{7}$$

where x_o is the unstretched node separation and m is the node mass. With the tethers attached at fixed locations on the spherical surfaces any rotation will result in a torque on the node. This is modeled to examine the correlations between translational and rotational motions. The attitude is governed by the rotational equation of motion:

$$\ddot{\theta} = -\frac{rk_s}{I}[x - x_o + 2r(1 - \cos\theta)]\sin\theta \tag{8}$$

where I is the mass moment of inertia of the node. For this 2DOF model the mass of each node is equal and the mass moment of inertia of a solid disk is used. Future studies can vary these properties to analyze the effect of mass and its distribution on the dynamics of the system.

B. Single-Tether Linearized Model

To focus on the dynamical motion of the nodes, the 2DOF model is linearized. Equation (7) has an equilibrium condition at a separation, $x = x_e$ and an attitude $\theta = 0$. At this equilibrium, the translational equation of motion is reduced to

$$\ddot{x} = 0 = \frac{k_c Q}{x_e^2} - k_s(x_e - x_o) \tag{9}$$

which can be arranged to a cubic relationship between the equilibrium distance x_e and the associated charge product Q:

$$k_c Q = k_s(x_e - x_0)x_e^2 \tag{10}$$

Of the three x_e solutions only the real solution is practical. At this equilibrium separation distance the Coulomb and tether forces are equal and the nodes remain stationary (with no external disturbances). One interesting consequence of this equilibrium distance is that it is independent of the system mass.

The 2DOF model given in Eqs. (7) and (8) is linearized about the equilibrium condition to produce a reduced system model to study the dynamic behavior of oscillations about the equilibrium states. Linearizing the translational motion for small departures ($\delta x = x - x_e$) results in:

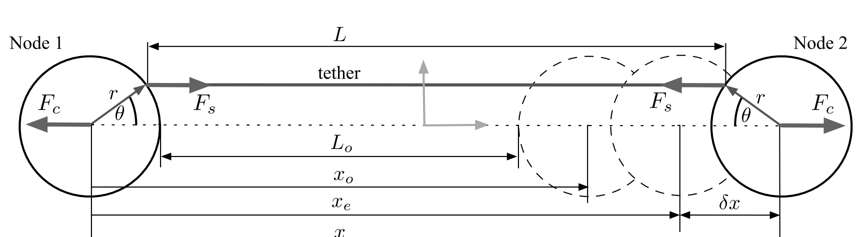

Fig. 5 Two-node system showing 2DOF motion through asymmetric rotations.

$$\delta\ddot{x} \approx -\frac{2}{m}\left[\frac{2k_c Q}{x_e^3(Q)} + k_s\right]\delta x \quad (11)$$

This approximate translation description is decoupled from the angular rotation and is the form of the stable, undamped harmonic oscillator equation. The natural frequency of this oscillatory translational response is given by

$$\omega_T = \sqrt{\frac{2}{m}\left[\frac{2k_c Q}{x_e^3(Q)} + k_s\right]} \quad (12)$$

The rotational equation of motion is linearized to the form

$$\ddot{\theta} \approx \frac{-rk_s}{I}[x_e(Q) - x_o]\theta \quad (13)$$

This linearized rotational equation of motion also decouples and is of the form of the stable undamped harmonic oscillator equation. The natural frequency of this oscillatory rotational response is given by

$$\omega_R = \sqrt{\frac{rk_s}{I}[x_e(Q) - x_o]} \quad (14)$$

While these linearized models are only valid for small oscillations, they can be used to offer insight into the response of the system about its equilibrium state.

V. Linearized Model Analysis

Using the linearized system model, two case studies are used to analyze motions and sensitivity to the nodal parameters; potential, tether material and separation. Ultimately, it is possible to gauge the expected stiffness of the TCS, with the linearized models of Eqs. (11) and (13) and using the system properties of Table 4.

A. Natural Frequency Response

The natural frequency of the linearized translational and rotational motions of Eqs. (12) and (14) gives a measure of the TCS stiffness. Figure 6 shows the natural frequency of the linearized translational motion for three separation distances. For the voltage range analyzed, the natural frequency of the response changes less than 0.1%, indicating that it is essentially independent of the spacecraft charge. The translational stiffness is largely determined by the tether material stiffness. As the separation distance between the nodes decreases, the frequency of the system response increases as a result of the shorter (stiffer) tethers and enhanced Coulomb force magnitudes.

Figure 7 shows the natural frequency of the linearized rotational motion, Eq. (14), for three separation distances. In contrast to the translational stiffness that is essentially decoupled from the magnitude of the electrostatic inflation force (assuming AmberStrand-like materials), the rotational stiffness or natural frequency is directly related to the TCS node potentials. The rotational natural frequency has a near-linear dependence on potential for the range of charges used in this study. In essence, the rotational motion will be stiffened through enhanced charge levels. Only for potentials much larger and unrealistic for spacecraft charging (>2000 kV) does the response become nonlinear.

Note that the translational natural frequency is at least 2 orders of magnitude greater than the corresponding rotational motion. For

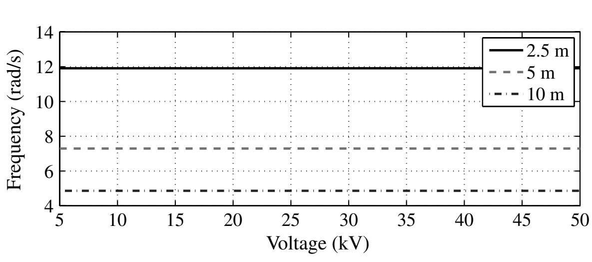

Fig. 6 Natural frequency of linearized translational motion.

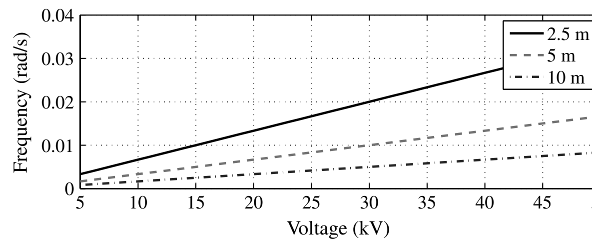

Fig. 7 Natural frequency of linearized rotational motion.

these uncoupled linearized equations and the system parameters analyzed, this implies that a TCS is naturally superior at constraining translational motion. Based on this outcome, the primary focus of this study is on the nodal rotational responses.

B. Sensitivity of Rotational Motion to Tether Material

AmberStrand is the example tether material used for this study. The use of an alternate tether material would change the material stiffness (spring constant). The linearized model is used to analyze the effect on the resulting rotational node motion by varying this tether material stiffness. Equation (13), which is the form of a stable oscillator, has the solution $\theta(t) = A\sin(\omega_R t + \beta)$, where β is the phase offset and the amplitude of the rotational response oscillation, A, is defined as

$$A = \dot{\theta}(0)\sqrt{\frac{2mr}{5}}\underbrace{\sqrt{\frac{1}{k_s(x_e(Q,k_s) - x_o)}}}_{\alpha} = \dot{\theta}(0)\sqrt{\frac{2mr}{5}}\alpha \quad (15)$$

Here, $\dot{\theta}(0)$ is the initial angular rate and $\theta(0)$ is assumed to be zero. The amplitude A is proportional to α, which is a function of the tether stiffness k_s and node charge product Q. Note that x_e depends on k_s so amplitude is not inversely proportional to the spring constant. For 10 m separated nodes tethered with the nominal AmberStrand braid the resulting spring constant value is $k_{s10} = 591$. This spring constant value corresponds to an amplitude factor α_{10}. Investigating the impact of the tether material properties is performed by varying the spring constant value from $k_{s10} \times 10^{-8}$ through $k_{s10} \times 10$. The resulting amplitude multiplication factor α of Eq. (15) is normalized by the nominal α_{10} value and plotted in Fig. 8 for a range of node potentials.

This study shows that changes in the tether spring constant have a minimal effect on the amplitude of angular rotations compared with the nominal 10 m separation (k_{s10}) response. It requires a spring constant that is reduced by 1×10^{-8} times the value of the 10 m separated case and nodes of 50 kV to increase the maximum angular rotation by only 2.5. Any tether material with a realistic spring constant or anything stiffer than the example tether material will result in the same rotational motion response, an important finding of the linearized analysis.

C. Extent of Linearization Range

The previous sections use linearized equations to analyze expected motions about equilibrium conditions. Numerical simulations using

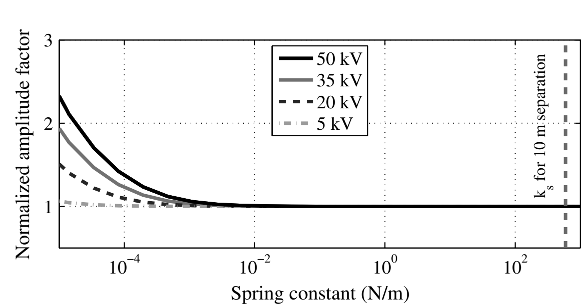

Fig. 8 Effect of varying tether spring constant on the amplitude of linearized angular oscillations.

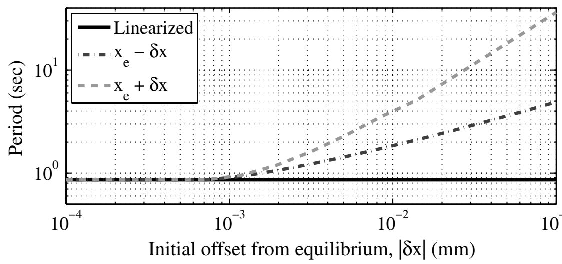

Fig. 9 Comparison of oscillation periods for linearized translational equation to nonlinear simulation.

the 2DOF model are used to quantify the extent of accuracy of these linear approximations. This is achieved by calculating the period of oscillation of the system response to deviations from equilibrium both with the translational and rotational equations of motion.

Figure 9 shows the period of oscillation of the two-node system initialized with a translational offset δx from equilibrium x_e. The period of oscillation is compared with that predicted from the linearized system of Eq. (12). The nodes are offset in both the compression and stretch directions ($x_e \pm \delta x$) and give different periods of oscillation. This figure indicates that the range of accuracy of the linearized translational equation is only $\pm 1 \times 10^{-3}$ mm.

Similarly, the period of oscillation of the two-node system initialized with a rotational offset $\delta\theta$ from the equilibrium angle of zero is shown in Fig. 10. The period of oscillation is compared with that predicted from the linearized system of Eq. (14). Because of symmetry, the nodes are offset only in the positive θ direction. This figure indicates that the range of accuracy of the linearized rotational equation is $\pm 8 \times 10^{-2}$ deg. Beyond this linear range the rotational oscillations abruptly change periods as the tether now becomes marginally slack at times causing the nodes to to lose their smooth rotations.

The conclusion of this study is that the linearization analysis only holds for very small departures from the respective equilibriums. The conclusions of the linearized analysis still hold and give insight into the expected performance of the TCS dynamics; However, the nonlinear nature of the TCS dynamics dominate, leading to the need for numerical simulations for further analysis.

VI. Numerical Simulation: Rotational Stiffness Capabilities

The linearized analysis gave an indication of the translational and rotational motions and their dependence on two key system parameters: craft potential and tether material. Because of the very nonlinear nature of TCS dynamics, further analysis of the rotational motion is conducted to demonstrate the TCS stiffening properties and capability to resist angular-rate errors.

After deployment, the TCS nodes will not be perfectly at rest with respect to each other. This analysis uses the full 3-D nonlinear equations of motion (see Appendix) to demonstrate the ability of the Coulomb force to stiffen the structure and resist deformation due to this initial angular rate. The two-node, single-tether TCS configuration with three different separation distances are simulated with asymmetric initial angular rotations. Here, both nodes perform

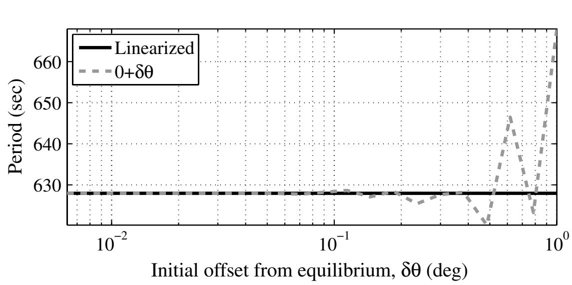

Fig. 10 Comparison of oscillation periods for linearized rotational equation to nonlinear simulation.

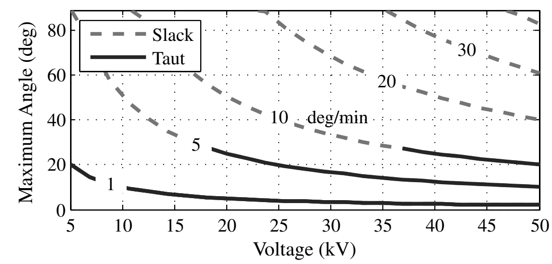

a) Maximum angle for 10 m separated nodes

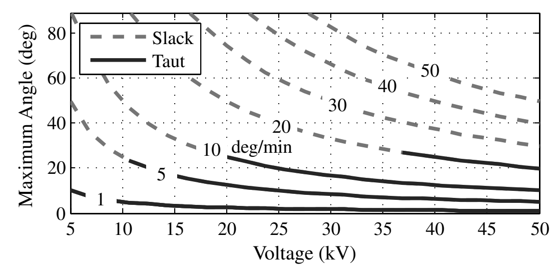

b) Maximum angle for 5 m separated nodes

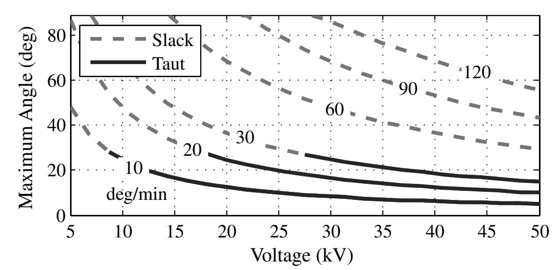

c) Maximum angle for 2.5 m separated nodes

Fig. 11 Maximum attitude reached as a function of initial attitude rate error.

the same (but opposite) rotation and, consequently, have one-dimensional translational motion, to focus on rotational dynamics.

Figure 11 shows the maximum attitude angle that is reached by the nodes for each of the separation distance cases. This is shown as a function of the spacecraft surface potential and each data line corresponds to the initial angular-rate error. No material damping is considered in this study as the focus is on the initial rotational response and issues with tethers wrapping up on nodes after a single oscillation. The weak material damping would only impact long-term oscillation amplitudes.

The solid lines in Fig. 11 indicate that the tether remains taut for the simulation duration, and the dashed regions have the tether reach a slack state. For many of these conditions the tether may go slack only a small fraction of the simulation time and is typically much less than a millimeter from the unstretched tether length. Given that there are only infrequent times of slight slackness, this is not a significant concern. It is anticipated that passive or active damping be added to the TCS system to assist the transient response to reach a taut tether equilibrium state. Future research investigating the use of active motion damping or passive damping with viscous materials at the tether attachment points is envisioned.

For the three separation cases analyzed the conditions that cause the angle of rotation to go above 27° results in a tether that will periodically go slack. Interestingly this rotation amplitude limit appears to be independent of the initial conditions considered or the node separations. The cause of this correlation is currently under investigation.

A reduction in the spacecraft separation distance results in two key changes on the system, as shown in Fig. 11. First, the tether spring constant increases; second, the spacecraft will be closer together, increasing the Coulomb force for an equivalent charge level. This increases the stiffening of the rotational motion, as preluded by the earlier linear analysis. This simulation now quantifies the enhanced

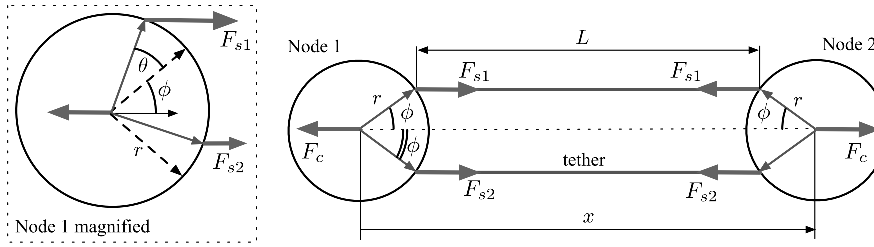

Fig. 12 Two-node system with double-tether.

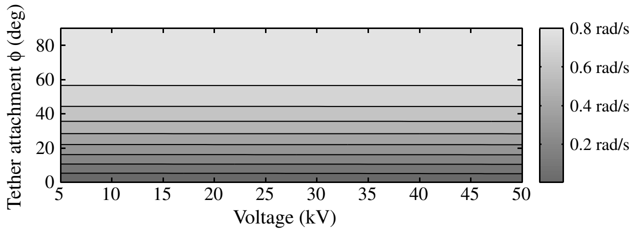

Fig. 13 Natural frequency of linearized rotational motion of double-tether model.

ability of a stiffened TCS to resist deformation due to an initial angular-rate error on the nodes. Figure 11a shows that a 10 m nodal separation with 35 kV potentials requires an initial nodal rotation rate less than 10 deg / min, a small value. Otherwise, the tethers will periodically go slack or the nodes could wrap up with the tethers. In contrast, Fig. 11c shows that reducing the separation to 2.5 m and maintaining a 35 kV potential will constrain a 45 deg / min angular rate. At these separations rates as high as 120 deg / min can be tolerated without nodal wrap-up. Shorter separation distances yield significant increases to the rotational stiffness of the TCS nodes.

VII. Double-Tether Rotational Stiffness Capabilities

Having a TCS system that incorporates a redundant set of tethers between the nodes, with the attachment points distributed across the nodes surface, is a method of increasing the rotational TCS node stiffness. The following numerical simulation results quantify by how much the rotational TCS node stiffness can be increased if a double-tether setup is employed.

A. Two-Degree-of-Freedom Model

The double-tether TCS concept is shown in Fig. 12 on a two-node system. The intent of the redundant double-tether is to add rigidity and resistance to deformation for the TCS. The system is modeled with asymmetric motions so that it can once again be reduced to 2 degrees of freedom to gain analytical insight.

The translational equations of motion of the symmetric double-tether system is

$$\ddot{x} = \frac{2k_c Q}{mx^2} - \frac{4k_s}{m}[x - x_o + 2r\cos\phi(1 - \cos\theta)] \tag{16}$$

where ϕ is the half-angle between the tether attachment points. The rotational equation of motion is given by

$$\ddot{\theta} = -\frac{2rk_s \sin\theta}{I}\{\cos\phi(x - x_o) + 2r[\cos\theta + \cos^2\phi - 2\cos\theta\cos\phi]\} \tag{17}$$

The rotational equation of motion is significantly more complex than the single-tether setup. However, linearizing the double-tether motions about the equilibrium states, still produces a decoupled set of equations. The translational motion for small departures about the equilibrium ($\delta x = x - x_e$) is

$$\delta\ddot{x} \approx -\frac{4}{m}\left[\frac{k_c Q}{x_e^3(Q)} + k_s\right]\delta x \tag{18}$$

This linearized translational motion is of the form of a stable undamped harmonic oscillator. It is also equivalent to the single-tether case of Eq. (11) with an additional factor of 2. This further increases the natural frequency and stiffness of the translational response. The rotational equation of motion is linearized to the form

$$\ddot{\theta} \approx \frac{-2rk_s}{I}[(x_e(Q) - x_o)\cos\phi + 2r(1 - \cos^2\phi)]\theta \tag{19}$$

This linearized rotational equation of motion decouples from the translational motion and is a stable undamped harmonic oscillator equation. Unlike the single-tether rotational motion of Eq. (13) this linearization features dependence on the tether attachment angle ϕ. Figure 13 plots the rotational natural frequency of Eq. (19) as a function of this tether attachment angle and potential. This figure shows how stiffening is significantly increased with the tether angle ϕ. This geometric stiffening is a consequence of the larger moment arm acting on the node. The data in this figure is generated with nodes of 0.5 m radius separated by 2.5 m. It should be noted that with zero tether separation ($\phi = 0$) the double-tether rotational natural frequency is equivalent to the single-tether system shown in Fig. 7.

Figure 7 showed for the single-tether case that increasing charge increases the natural frequency of the rotational response. This also occurs with the natural frequency of the double tether shown in Fig. 13; however, it has less contribution than the geometric stiffening. Using a double tether will increase the ability to resist nodal angular rotations.

B. Double-Tether System Response to Angular-Rate Errors

In this simulation case the double-tether response to angular-rate errors is compared with that of a single-tether configuration. A two-node configuration with a separation of 2.5 m is analyzed. The simulation is performed using the full 3-D and nonlinear coupled equations of motion. The parameters of the symmetric simulation are shown in Table 5.

Using two initial angular-rate errors for each tethered system the resulting maximum attitude angle reached is shown in Fig. 14 on a y-axis log plot. There is a noticeable difference in the systems responses. The double-tether system performs better at reducing maximum rotation due to initial rate errors. This indicates that the resulting moment arm from the double-tether configuration significantly increases the system's response to angular rates. While the double-tether system has the advantage of producing a stiffer system, it is also prone to having a tether go slack, as shown by the dashed lines in the figure. The tether is only marginally and momentarily slack at times of closest approach between the nodes. Once again, during these times the tether is slack less than 1 mm over

Table 5 Double-tether simulation parameters

Parameter	Value	Units
Initial attitude rate errors $\dot{\theta}(0)$	5,10	deg / min
Spacecraft node radius r	0.5	m
Spacecraft separation x_o	2.5	m
Tether attachment point angle ϕ	20	deg

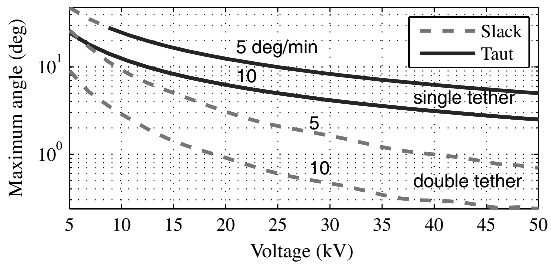

Fig. 14 Double-tether vs single-tether attitude response to angular-rate errors.

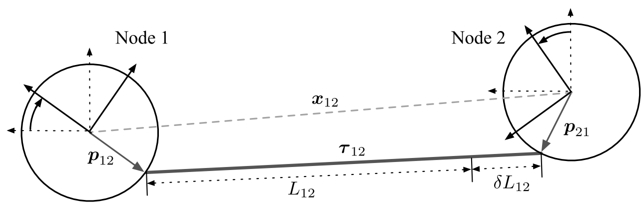

Fig. 15 Two-node example of attitude change and increased tether length.

its entire length. In contrast, during this simulation case the single-tether system remains taut for any charge above 10 kV, at a cost of reaching higher attitude angles. Another consideration with the double-tether TCS is that the nodes are inherently closer to wrap-up due to the tether connection angle. A comparison between the resistance to absolute angular rotation versus the close proximity to wrap-up must be considered.

The results of this preliminary double-tether simulation indicate that a TCS system can be significantly stiffened beyond an equivalent single-tether system. This offers enhanced capabilities to resist torque disturbances or deployment motions. An additional advantage is the safety provided by having two tethers between nodes. In case one tether is severed, the remaining tether would still maintain the TCS shape, although with reduced accuracy.

VIII. Conclusions

The novel TCS concept offers unique on-orbit advantages. Large space structures are envisioned that can be launched in a low-mass and compact configuration and deployed and resized once on-orbit. To advance the concept, this study analyzes the coupling between relative translational and rotational motions of the tethered spacecraft nodes. A baseline two-node TCS system is the focus of this study.

Numerical results obtained with the full three-dimensional nonlinear equations of motion indicate that external perturbations such as SRP or differential gravity have minimal influence on the short-term dynamics. For obtainable kilovolt level potentials the TCS system will sufficiently inflate and resist deformation from external forces. This is shown first through simplified linearized models that give an analytical expression for the natural frequency of isolated translation and rotational motions. The natural frequency is an indication of the stiffness of the system and the rotational motions offer lower values and are the focus of this study. The TCS rotational response to initial angular-rate errors is also quantified and shown to significantly improve with the use of an additional tether.

This versatility of the numerical simulation and ability to examine any general N-node TCS system will be advantageous in future TCS studies where more complex networking is considered. This two-node study considers a worst-case situation in which the tether network provides minimal rotational stiffening. Multitether connections to a node, such as with a three-node triangular system, will provide increased rotational stiffness. This concept is illustrated in this study by investigating the multitether connection among two nodes. Future studies will investigate three-dimensional TCS configurations as well as incorporate low-tension behavior models.

Appendix: Three-Dimensional TCS Modeling

The simplified 2DOF TCS models offer insight into translational and rotational motion. Shown here is the development of the full three-dimensional nonlinear equations of motion that can accommodate general TCS spacecraft configurations. The algorithm simulates the TCS in deep space or under the gravitational attraction of orbit and incorporates external disturbance forces, such as SRP. Although not performed in this study, the intent of this algorithm is to fully explore the capabilities and operating regimes of the TCS along with a study of its dynamic behavior under realistic disturbance environments. The algorithm can perform TCS relative motion studies accommodating any number of nodes and tethers in any initial orbit configuration.

The location of each spacecraft node, $\boldsymbol{R}_i$, is defined in an Earth-centered inertial frame. At epoch, the body frame alignment and nominal separation distances of each node is defined. The equations are shown here for nodes connected with just a single tether that has a fixed attachment point on the spherical surfaces. It is not necessary to have a tether connecting each node as a tether connection matrix, $[K_{ij}]$, defines which nodes are connected. The tethers are modeled as linear springs and can stretch from either the nodal relative motion or from attitude rotations, as shown in Fig. 15. The resulting tensile force acting on node i from the tether connected to node j is

$$\boldsymbol{T}_{ij} = k_s \delta L_{ij} \hat{\boldsymbol{\tau}}_{ij} \tag{A1}$$

where $\boldsymbol{\tau}_{ij}$ is the vector defining the tether connecting node i to j. When the tether length is shorter than desired, the tether goes slack and there is no force acting on the corresponding nodes.

A. Translational Equation of Motion

Using the Coulomb force of Eq. (1), tensile force and the gravitational force, the resulting equations of motion of each node is calculated using

$$\ddot{\boldsymbol{R}}_i = -\frac{\mu}{|\boldsymbol{R}_i|^2}\hat{R}_i + \sum_{j=1}^{N} K_{ij}\frac{\boldsymbol{T}_{ij}}{m_i} + \sum_{j=1}^{N}\frac{k_c q_i q_j(-\hat{\boldsymbol{x}}_{ij})}{m_i x_{ij}^2} e^{-x_{ij}/\lambda_d}\left(1+\frac{x_{ij}}{\lambda_d}\right) + \boldsymbol{F}_{\mathrm{SRP}} \quad i \neq j \tag{A2}$$

where $\mu = 3.986 \times 10^{14}\ \mathrm{m^3\,s^{-2}}$ is the gravitational coefficient for Earth, m_i is the spacecraft node mass, N is the total number of nodes in the TCS model, and K_{ij} is a scalar based on the adjacency matrix, which is 0 if no tethers connected or 1 if any tethers are connected. Note that these charges do not influence the relative motion. They simply provide an inflating force, relative to the systems center of mass, that increases the tether tensions. In addition, the Coulomb force is calculated based on a point charge approximation, even though the nodes have a distributed surface charge. The motion of each node is propagated in time using a variable step Runge-Kutta algorithm.

B. Nodal Rotational Equation of Motion

The attitude of each spacecraft node is also propagated by computing the torque acting on the node from each tether:

$${}^{\mathcal{B}}\Gamma_i = \sum_{j=1}^{N}(K_{ij}^{\mathcal{B}}\boldsymbol{p}_{ij} \times [\mathcal{BI}]_i^{\mathcal{I}}\boldsymbol{T}_{ij}), \quad i \neq j \tag{A3}$$

where $\boldsymbol{p}_{ij}$ is the body fixed vector that defines the location of the tether connection point on node i that connects to node j and $[\mathcal{BI}]_i$ is the direction cosine matrix of the attitude of node i relative to the inertial frame. The angular acceleration of each node is defined in the body frame with Euler's rotational equations of motion [32]:

$$[I]\dot{\boldsymbol{\omega}}_i = -\boldsymbol{\omega}_i \times ([I]\boldsymbol{\omega}_i) + \Gamma_i \tag{A4}$$

The attitude of each node is represented with the modified Rodrigues parameters (MRP), which are integrated using the differential kinematic equation:

$$\dot{\boldsymbol{\sigma}}_i = \frac{1}{4}[(1-\sigma_i^2)[I_{3\times 3}] + 2[\tilde{\boldsymbol{\sigma}}]_i + 2\boldsymbol{\sigma}_i\boldsymbol{\sigma}_i^T]\boldsymbol{\omega}_i \tag{A5}$$

The MRP set will go singular with a rotation of $\pm 360°$. To ensure a nonsingular description, the MRP description is switched to the shadow set whenever $|\boldsymbol{\sigma}| > 1$ [32].

Acknowledgment

The authors would like to thank the Aerospace Engineering Sciences senior design team of the CubeSat Tether System for the AmberStrand material properties.

References

[1] Freeland, R. E., Bilyeu, G. D., Veal, G. R., and Mikulas, M. M., "Inflatable Deployable Space Structures Technology Summary," *49th International Astronautical Congress*, Melbourne, Australia, 1998.

[2] Cobb, R. G., Lindemuth, S. N., Slater, J. C., and Maddux, M. R., "Development and Test of a Rigidizable Inflatable Structure Experiment," 45th AIAA/ASME/ASCE/AHS/ASC Structures, Structural Dynamics & Materials Conference, AIAA Paper 2004–1666, Palm Springs, CA, April 2004.

[3] Tarazaga, P. A., Inman, D. J., and Wilkie, W. K., "Control of a Space Rigidizable Inflatable Boom Using Macro-Fiber Composite Actuators," *Journal of Vibration and Control*, Vol. 13, No. 7, 2007, pp. 935–950.
doi:10.1177/1077546307078757

[4] Fang, H., Knarr, K., Quijano, U., Huang, J., and Thomson, M., "In-space Deployable Reflectarray Antenna: Current and Future," AIAA/ASME/ASCE/AHS/ASC Structures, Structural Dynamics and Materials Conference, Schaumburg, IL, AIAA Paper 2008-2209, April 2008.

[5] Carpenter, K. G., Schrijver, C. J., Karovska, M., and Team, S. M. C. D., "The Stellar Imager (SI) Project: A Deep Space UV/Optical Interferometer (UVOI) to Observe the Universe at 0.1 Milli-Arcsec Angular Resolution," *Proceedings of the NUVA Conference*, El Escorial, Spain, June 2007.

[6] Blackwood, G., Henry, C., Serabyn, E., Dubovitsky, S., Aung, M., and Gunter, S. M., "Technology and Design of an Infrared Interferometer for the Terrestrial Planet Finder," AIAA Space 2003, AIAA Paper 2003-6329, Long Beach, CA, Sept. 2003.

[7] Wertz, J. R., "High Resolution Structureless Telescope," NASA Institute for Advanced Concepts, Final Report, TR MC04-1643, April 2004.

[8] Hyde, R., Dixit, S., Weisberg, A., and Rushford, M., "Eyeglass: A Very Large Aperture Diffractive Space Telescope," *Proceedings of SPIE*, Vol. 4849, 2002, pp. 28–39.
doi:10.1117/12.460420

[9] Hyde, R., "Eyeglass Large Aperture, Lightweight Space Optics," Lawrence Livermore National Lab., TR. UCRL-ID- 151390, Livermore, CA, Feb. 2003.

[10] King, L. B., Parker, G. G., Deshmukh, S., and Chong, J.-H., "Spacecraft Formation-Flying Using Inter-Vehicle Coulomb Forces," NASA Institute for Advanced Concepts, Final Report, Jan. 2002.

[11] Miller, D. W., Sedwick, R. J., Kong, E. M. C., and Schweighart, S., "Electromagnetic Formation Flight for Sparse Aperture Telescopes," *IEEE Aerospace Conference Proceedings—Volume 2*, IEEE Press, Piscataway, NJ, March 2002, pp. 2-729–2-741.

[12] Gersh, J., "Architecting the Very-Large-Aperture Flux-Pinned Space Telescope: A Scalable, Modular Obtical Array with High Agility and Passively Stable Orbital Dynamics," AAS/AIAA Astrodynamics Specialist Conference, Honolulu, HI, AIAA Paper 2008-7212, Aug. 2008.

[13] Seubert, C. R., and Schaub, H., "Tethered Coulomb Structures: Prospects and Challenges," *F. Landis Markley Astrodynamics Symposium*, American Astronautical Society, Paper 08–269, Cambridge, MA, 2008.

[14] King, L. B., Parker, G. G., Deshmukh, S., and Chong, J.-H., "Study of Interspacecraft Coulomb Forces and Implications for Formation Flying," *Journal of Propulsion and Power*, Vol. 19, No. 3, May–June 2003, pp. 497–505.
doi:10.2514/2.6133

[15] Natarajan, A., and Schaub, H., "Linear Dynamics and Stability Analysis of a Coulomb Tether Formation," *Journal of Guidance, Control, and Dynamics*, Vol. 29, No. 4, July–Aug. 2006, pp. 831–839.
doi:10.2514/1.16480

[16] Natarajan, A., Schaub, H., and Parker, G. G., "Reconfiguration of a Nadir-Pointing 2-Craft Coulomb Tether," *Journal of the British Interplanetary Society*, Vol. 60, No. 6, June 2007, pp. 209–218.

[17] Tragesser, S. G., and Tuncay, A., "Orbital Design of Earth-Oriented Tethered Satellite Formations," *Journal of the Astronautical Sciences*, Vol. 53, No. 1, Jan.–March 2005, pp. 51–64.

[18] Menon, C., and Bombardelli, C., "Self-Stabilising Attitude Control for Spinning Tethered Formations," *Acta Astronautica*, Vol. 60, 2007, pp. 828–833.
doi:10.1016/j.actaastro.2006.11.013

[19] Beletsky, V. V., and Levin, E. M., *Dynamics of Space Tether Systems*, Advances in the Astronautical Sciences, Vol. 83, American Astronautical Society, Springfield, VA, 1993, pp. 20–25.

[20] Cosmo, M. L., and Lorenzini, E. C., "Tethers in Space Handbook," 3rd ed., NASA Marshall Space Flight Center, Dec. 1997.

[21] Berryman, J., and Schaub, H., "Static Equilibrium Configurations in GEO Coulomb Spacecraft Formations," AAS/AIAA Spaceflight Mechanics Meeting, American Astronautical Society Paper 05–104, Copper Mountain, CO, Jan. 2005.

[22] Vasavada, H., and Schaub, H., "Analytic Solutions for Equal Mass Four-Craft Static Coulomb Formation," *Journal of the Astronautical Sciences*, Vol. 56, No. 1, Jan.–Mar. 2008, pp. 17–40.

[23] Natarajan, A., and Schaub, H., "Hybrid Control of Orbit Normal and Along-Track 2-Craft Coulomb Tethers," AAS/AIAA Spaceflight Mechanics Meeting, American Astronautical Society Paper 07–193, Sedona, AZ, 2007.

[24] Wang, S., and Schaub, H., "One-Dimensional 3-Craft Coulomb Structure Control," *7th International Conference on Dynamics and Control of Systems and Structures in Space*, London, July 2006, pp. 269–278.

[25] Wang, S., and Schaub, H., "Switched Lyapunov Function Based Coulomb Control of a Triangular 3-Vehicle Cluster," AAS/AIAA Astrodynamics Specialist Conference, Pittsburgh, PA, American Astronautical Society, Paper AAS-09-391, Aug. 2009.

[26] Gombosi, T. I., *Physics of the Space Environment*, Cambridge Univ. Press, New York, 1998.

[27] Schaub, H., Parker, G. G., and King, L. B., "Challenges and Prospect of Coulomb Formations," *Journal of the Astronautical Sciences*, Vol. 52, No. 1–2, Jan.–June 2004, pp. 169–193.

[28] Valk, S., Lemaitre, A., and Deleflie, F., "Semi-Analytical Theory of Mean Orbital Motion for Geosynchronous Space Debris Under Gravitational Influence," *Advances in Space Research*, Vol. 43, No. 7, 2009, pp. 1070–1082.
doi:10.1016/j.asr.2008.12.015

[29] Vallado, D. A., *Fundamentals of Astrodynamics and Applications*, 3rd ed., Space Technology Library, Springer, New York, 2007.

[30] Katz, I., Jongeward, G. A., Davis, V. A., Mandell, M. J., Kuharski, R. A., Lilley, J. R., Jr., et al., "Structure of the Bipolar Plasma Sheath Generated by SPEAR I," *Journal of Geophysical Research*, Vol. 94, No. A2, Feb. 1989, pp. 1450–1458.
doi:10.1029/JA094iA02p01450

[31] Olsen, R. C., Van Horn, T., Torbert, R., and Raitt, W. J., "SPEAR-1 Charging Behavior," *ESA Space Environment Analysis Workshop*, Oct. 1990.

[32] Schaub, H., and Junkins, J. L., *Analytical Mechanics of Space Systems*, 2nd ed., AIAA Education Series, AIAA, Reston, VA, Oct. 2009.

G. Agnes
Associate Editor